UDK 621.396

A COMPETITIVE DESCRIPTIVE REGULARIZATION MVDR BEAMFORMING APPROACH FOR FEATURE ENHANCED ARRAY RADAR IMAGING

YURIY SHKVARKO, VICTOR ESPADAS, AND DAVID CASTRO

The paper develops a new robust adaptive beamforming (AB) inspired approach for high resolution array radar imaging in harsh sensing environments. At the hardware codesign level, i.e., the array configuring stage, we adopt the celebrated GeoSTAR sensor array geometry that provides a desirable low side lobes level of the point spread function (PSF) attained employing the conventional matched spatial filtering (MSF) technique for radar image formation. At the software codesign level, i.e., the algorithm design stage, we suggest performing the unification of the recently developed descriptive experiment design regularization (DEDR) framework with the sparsity preserving and convergence guaranteed regularizing projections onto convex solution sets (POCS). The low resolution MSF image serves as an input (zerostep iteration) for the feature enhancing DEDRPOCSAB processing. The latter is implemented in an effective implicit iterative fashion avoiding cumbersome data covariance matrix inversions in contrast to all competing minimum variance distortionless response (MVDR) inspired robust ABbased radar imaging techniques. The effectiveness of the proposed method in comparison with the most prominent competing techniques is corroborated via extended simulations adapted for the harsh test sensing scenarios of multiple target imaging with mmband array radar systems that employ different feasible sensor array configurations.

Keywords: antenna array, descriptive experiment design, imaging radar, iterative processing, regularization.

INTRODUCTION

Beamforming is a pervading task in a variety of array radar signal processing applications, (e.g., see [1] – [11] and the references therein), in particular, in feature enhanced array radar imaging (RI) that is a matter of this study. Due to adaptive (i.e., structurally constrained data dependent) adjustment of the weight vectors in the processing array radar channels the adaptive beamforming (AB) based RI techniques can attain enhanced resolution performances and much better interference rejection capability than the data-independent beamformers that implement the conventional so-called matched spatial filtering (MSF) image formation method [2], [6]. However the AB-based techniques are sensitive to harsh operational scenario uncertainties attributed to random signal perturbations in a turbulent propagation medium, possible imperfect sensor array system calibration, signal fading, near-far waveform mismodeling, local scattering, multiplicative noise, angular spreading, as well as other distorting effects. In such harsh practical scenarios, the performance degradation of the traditional MVDR inspired AB-based techniques become pronounced because most of these techniques are based on the assumption of an accurate knowledge of the array response of the desired signal [6]. The problem has spurred development of various robust AB versions, and many sophisticated robust AB techniques are now available including the considered RI applications (e.g., see [2]–[4], [7]–[11] and the references therein). The majority of those employ the robust modifications of the celebrated MVDR method [2], [9]–[11] that all require cumbersome data covariance matrix inversions. Different robust AB versions adapted for harsh sensing scenarios propose specific procedures based on the so-called worst-case performance optimization [2], [6] that also employs cumbersome matrix inversions. Crucial still unresolved problem relates to the development of robust AB-based feature enhanced RI framework and related techniques that avoid such cumbersome data covariance matrix inversions proposing alternative approaches based on imaging inverse problem phenomenology and employing multilevel image formation concepts with iterative reconstructive radar image processing.

In the previous paper of this series [1], we have featured the descriptive experiment design regularization (DEDR)-based approach [8], [9] for robust imaging of multiple target scenes via space-time processing of multimode mm-band array radar data. The multiple frequency-polarization signal processing (SP) mode was employed to provide necessary DEDR redundancy that was next exploited to enhance the spatial resolution performances in different operational environments including harsh scenarios with imperfect array calibration, partial sensor failure and/or uncertain noise statistics. The addressed in [1] framework can be referred to as a robust extension of the Van-Cittert-Zernike approach [5], [11] based on the matched spatial filter bank SP for such realistic operational scenarios. Hence, the MSF-based low resolution array radar image formation employs the robust regularized matched spatial filter bank SP [1]. At the hardware (HW) co-design level (i.e., the array configuring) we adopted the celebrated Geo-synthesized thinned array radiometer (GeoSTAR) sensor array geometry [5]. In [1], the HW co-design problem of suppression of the sidelobes in the resulting MSF system output point spread function (PSF) balanced over the minimization of the effective width of its principal lobe was resolved by optimizing the array configuration characteristics. As it was featured in [1], the advantage of the GeoSTAR array geometry consists in providing a desirable PSF shape with a sharp principal lobe and considerably lower side lobes level than those attained with other feasible array configurations [1], [2], [5]. Unfortunately, being robust against harsh scenario model uncertainties, such DEDR-related MSF imaging technique provides images that do not manifest enhanced spatial resolution performances because no structurally constrained robust AB-based SP and image processing have been employed.

In this paper we address a new robust AB-based approach for high resolution array radar imaging in harsh sensing scenarios. At the software (SW) co-design, i.e., the algorithm design level, the new robust AB-based RI technique utilizes the idea of unification of the recently developed robust DEDR framework [9], [16] with the sparsity preserving and convergence guaranteed regularizing projections onto convex solution sets (POCS) [11]. As in the previous developments [1], at the HW co-design level we adopt the celebrated GeoSTAR sensor array configuration [5]. The feature enhanced RI is next stated and treated in the context of imaging inverse problems phenomenology [11], [16], [18]. In the addressed framework, the MSF image serves as an input (zero-step iteration) for the second level feature enhanced reconstructive imaging via multilevel DEDR-POCS-AB-based processing of the initial low resolution MSF image. The reconstructive feature enhanced image processing is implemented in an effective implicit iterative fashion avoiding cumbersome data empirical covariance matrix inversions in contrast to all considered competing minimum variance distortionless response (MVDR) based robust AB techniques, e.g., [2], [6], [13], [14]. The effectiveness of the proposed method in comparison with other most prominent competing RI techniques [2], [6], [14] is corroborated via extended simulations adapted for the test scenarios of multiple target imaging with mm-band array radar systems that employ different sensor array configurations [1]. The results are indicative of the superior operational efficiency of high resolution localization of the multiple closely spaced targets with the GeoSTAR configured array imaging radar that implements the proposed multilevel DEDR-POCD-AB signal processing method.

The rest of the paper is organized as follows. In Sections I and II we recall the main HW-SW co-design results of the DEDR-related MSF method referring to the first paper of these series [1]. Section III presents the imaging inverse problem formalism of the feature enhanced RI problem at hand. In Section IV we develop our new DEDR-POCS-restructured MVDR approach that leads to the DEDR-POCS-AB framework. The implicit iterative scheme for efficient implementation of the overall DEDR-POCS-AB technique for feature enhanced array radar imaging that do *not* involve *any* matrix inversions is detailed in Section V followed by the simulation results with the relevant discussions in Section VI and concluding remarks in Section VII.

I. CONSIDERED RI SYSTEM HW SPECIFICATIONS

The GeoSTAR imaging sensor system has been originally addressed in [5] as a concept to provide high resolution imaging of distributed scenes remotely sensed with passive microwave and mm waveband radiometers. Nevertheless, the celebrated GeoSTAR array configuration is also well adapted for active RI systems as it was demonstrated in [15] and also featured in details in the previous study [1]. The particular mm-band imaging array radar system considered in that previous paper [1] is a multimode array sensor system. Such system operates at two separate yet concurrent frequencies of 24.5 GHz and 35 GHz with dual polarization (V – vertical and H – horizontal). At one instant, radio frequency (RF) pulses of a specified very narrow (~10 ns) pulse width (PW) are transmitted concurrently at 24.5 and 35 GHz in either V polarization or H polarization. These pulses are “calibrated” to maintain coherency so that their amplitudes and phases are constant for different pulses. The transmitting antenna is switched between vertical (V) and horizontal (H) polarizations, i.e., V and H transmitted pulses are delayed by a certain time. For each frequency (24.5 GHz or 35 GHz), transmitted V polarized and H polarized RF pulses are separated by a half of the fixed pulse repetition time (PRT/2).

In [1], the antenna array is composed of 24 elements as in [5], [15]. Each sensor element receives signals at V and H polarizations. The received signals are spread over time duration of $N = R_r$ PWs, where R_r is the number of range resolution cells used to process the received signals for each transmitted pulse. In every PRT corresponding to one frequency band (24 GHz or 36 GHz), one time delay vector $\mathbf{T}_\mathrm{d}$ and 4 measurement data vectors, $\{\mathbf{u}_{\mathrm{VV}}, \mathbf{u}_{\mathrm{VH}}, \mathbf{u}_{\mathrm{HV}}, \mathbf{u}_{\mathrm{HH}}\}$ are provided for further processing. That is, for each polarization mode {VV, VH, HV, HH} there is no time delay between receiving antenna elements since they are spaced close to each other, so $\mathbf{T}_\mathrm{d}$ has the same value for all 24 array elements for each range gate. Next, each data vector in the set $\{\mathbf{u}_{\mathrm{VV}},..., \mathbf{u}_{\mathrm{HH}}\}$ contains the relevant in phase (I) and quadrature (Q) components that compose 24-element (m = 1,..., 24) data vectors collected for $2R_r$ measurement time instants. The operation range of the system lies in the interval from 1m to 50m, with a range resolution cell of 0.3m, so at the SP level the observer controls R_r = 165 overall processing range gates.

The crucial SP issue relates to the formation of the empirical estimate $\mathbf{Y}_{r|p} = \underset{j}{aver}\{\mathbf{u}_{r|p}(j)\mathbf{u}^{+}_{r|p}(j)\}$ of the sensor data true correlation matrix $\mathbf{R}_{r|p} = <\mathbf{u}_{r|p}\mathbf{u}^{+}_{r|p}>$ for each range gate r = 1, ..., R_r = 165 at each polarization mode indexed now by p = VV, VH, HV, HH. The independent realizations $\{\mathbf{u}_{r|p}(j);\ j=1,...,J\}$ in the averaging procedure for formation of $\mathbf{Y}_{r|p}$ are to be recorded over J transmitted pulses for each range gate r at each polarization mode p. To guarantee the full-rank sensor data covariance matrices $\{\mathbf{Y}_{r|p};\ r$ = 1,...,

$R_r = 165$; $p = 1,..., 4\}$ the minimal number of independent recordings J should be not less than the number of sensors ($M = 24$), thus $J > 24$ independent realizations are to be recorded for each feasible "range gate (r) – polarization mode (p)" combination $\{r|p\}$. In the opposite case ($J < 24$), the empirical data covariance matrices are rank-deficient. This means that for $J < 24$ at the corresponding $\{r|p\}$ the robust MSF-based beamforming inevitably faces the problem of huge artifacts on the low resolution noise corrupted scene images [11], [18]. At the target detection SP stage, such artifacts inevitably increase the false alarm rate [2], [6], [11], [14]. That is why, in all SP developments in [1] and in this study, the redundancy guaranteed data collection mode $J > 24$ is considered.

To compare different HW designs, in [1] we featured three feasible sensor array configurations. Fig. 1(a) shows the conventional X-shaped equally spaced 24 element antenna array layout for the inter-element spacing $d_A = 1.8\lambda_o$, where λ_o defines the employed wavelength, in this case $f_o = 24$ GHz. The corresponding so-called *uv* spatial samples in the *visibility* domain are presented in Fig. 1(b). In Fig. 2(a), a circular-shaped (O-shaped) antenna array layout with the same parameters is depicted. The related *uv* spatial visibility samples are shown in Fig. 2(b). The GeoSTAR Y-shaped array layout is presented in Fig. 3(a) with the corresponding *uv* samples in Fig 3(b), respectively. In all cases, u and v samples specify the normalized (so-called *visibility* domain) coordinate representation format, i.e., $u = x/\lambda_o$, and $v = y/\lambda_o$.

II. MSF IMAGE FORMATION TECHNIQUE

The DEDR-related (i.e., low artifacts) MSF-based image formation algorithm featured in the previous study [1] comes directly from the Celebrated Van-Cittert-Zernike theorem from radio astronomy [5], [11] according to which, the noise-free data visibility function $R(u,v)$ (constructed directly from the noise free data true covariance function $R(x,y)$ at each range gate via its scaling to the visibility domain [11]) and the related spatial spectrum pattern (SSP) or the angular brightness distribution $b(\theta_x,\theta_y)$ over the 2-D angular observation space $(\theta_x,\theta_y)\in\Theta$ are related through the 2-D spatial inverse Fourier transform [1]

$$R(u,v) = c\Im_\theta^{-1}\{b(\theta_x,\theta_y)\} = = c\int_\Theta b(\theta_x,\theta_y)\exp\left[+i2\pi(u\theta_x+v\theta_y)\right]d\theta_x\,d\theta_y \qquad (1)$$

where c is the normalizing constant (not critical for image formation and analysis) and the visibility function arguments (u,v) represent the x-y projections of the normalized sensor baseline vectors (normalized to the wavelength λ_o) in the visibility domain $(u, v) \in \mathrm{P}/\lambda_o$ [1], [5]. Also, starting from (1) and all over the remained paper text we omit the range (r) – polarization (p) subscripts standing with $R(u,v)$, $R(x,y)$ and the related matrix-form representations **R**, **Y**, because the developed further theory and implementation techniques for spatial (over angular variables $(\theta_x,\theta_y)\in\Theta$) resolution enhanced imaging is similar for all range gates, $r = 1, ..., R_r$ and all employed polarization modes, $p = \{\mathrm{VV, VH, HV, HH}\}$. Thus, in the following developments of the conventional MSF and spatially enhanced reconstructive array radar imaging techniques, any particular feasible "range gate (r) – polarization mode (p)" combination $\{r|p\}$ can be assumed.

The robust MSF-based method for low resolution image formation featured in [1] implies, first, formation of the observed noised visibility function $\hat{R}(u,v)$ via scaling the estimated correlation matrix **Y** to the visibility domain (over the range of normalized visibility spacings $(u,v)\in\mathrm{P}/\lambda_o$) followed, second, by the 2-D Fourier transform that yields the MSF image of the scene

$$\hat{b}(\theta_x,\theta_y) = \Im_{u,v}\left\{\Pi_{A(u,v)}\,\hat{R}(u,v)\right\} = = \int_{\mathrm{P}/\lambda_0}\Pi_{A(u,v)}\,\hat{R}(u,v)\exp\left[-i2\pi(u\theta_x+v\theta_y)\right]du dv \qquad (2)$$

at a particular feasible $\{r|p\}$ combination [1]. Here, $\Im_{u,v}$ denotes the 2-D Fourier transform operator over $(u,v) \in \mathrm{P}/\lambda_o$ coordinates, and $\Pi_{A\{u,v\}}$ defines a projector that specifies the particular employed sensor array configuration resulting in different resolution performances attainable with the MSF-based imaging technique (2). In the pursued in [1] nonparametric RI problem treatment, the spatial resolution quality is assessed by the shape of the resulting MSF system PSF associated with the image (2) of a single point-type target (TAG) located at the origin of the scene coordinate system at the corresponding range gate $r\in R$ and relevant polarization mode p. In particular, the desired system PSF is associated with a shape that provides the lowest possible side lobes (and grating lobes) level balanced over the minimum achievable effective width of the PSF's main (principal) lobe [1], [2], [11], [14]. The feasible array configurations featured in [1] encompass the conventional X-shaped and O-shaped arrays [15] and the GeoSTAR-configured Y-shaped array [5]. Figures 1(c), 2(c) and 3(c) present the PSFs provided by the MSF single TAG imaging procedure (2) employing projectors $\Pi_{A\{u,v\}}$ related to the cross-shaped (X-shaped) [15], circular-shaped (O-shaped) [15] and the GeoSTAR-configured Y-shaped sensor array [1], [5] geometries, respectively. Note that the spatial resolution performances attained with the 2-D FFT MSF technique (2) are characterized by the width of the PSF's principal lobe and the maximum level of its secondary lobes (including the suppressed grating lobes). The corresponding PSFs computed using the simulations SW developed in [1] are reported in Figures 1(c)–3(c). Those corroborate that the Y-shaped GeoSTAR configured array outperforms two other feasible conventional (X-shaped and O-shaped) array configurations [1].

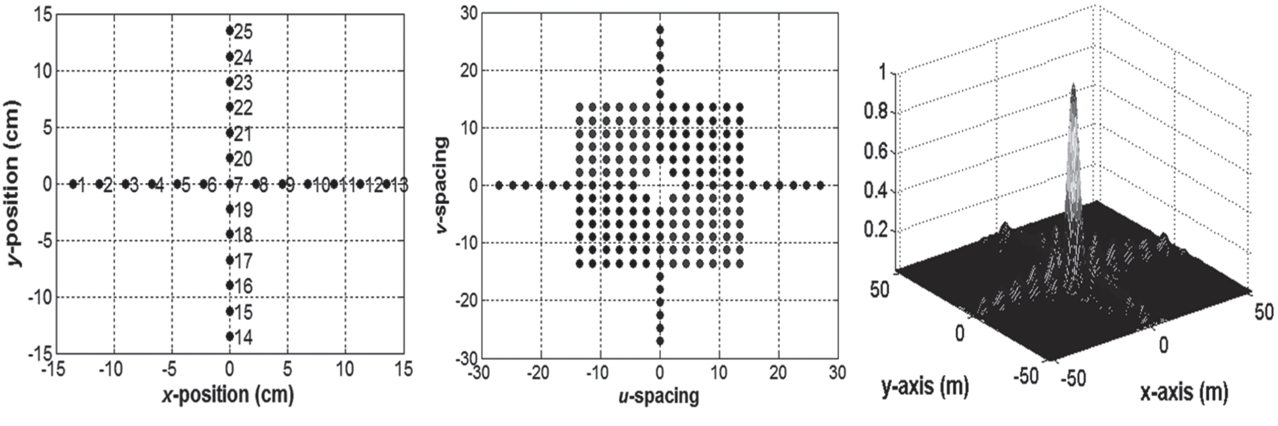

(a) (b) (c)

Fig. 1. (a) Antenna array layout with sensors numbering for X-shaped configuration;
(b) corresponding *uv* samples for inter-element spacing $d_A = 1.8\lambda_o$; carrier frequency $f_o = 24$GHz;
(c) relevant PSF for 24 element X-shaped configured imaging array

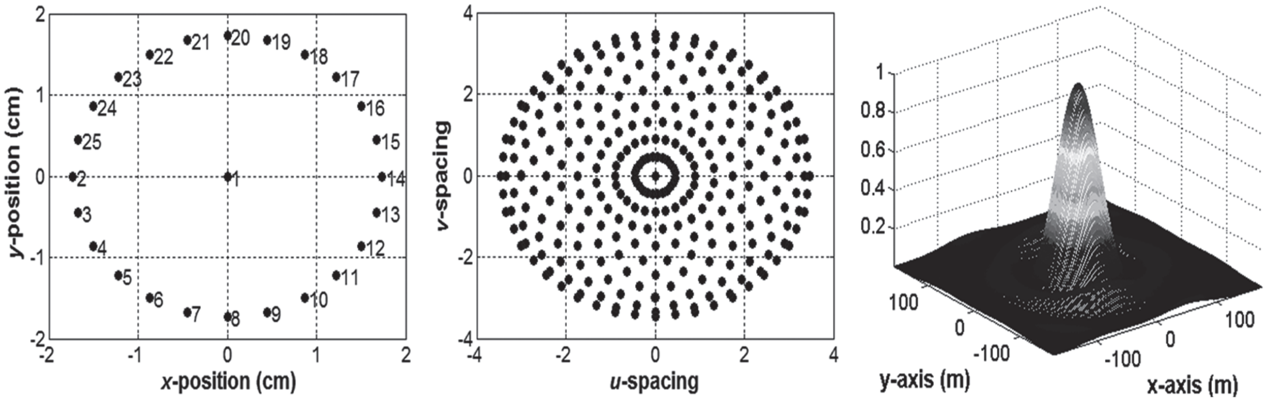

(a) (b) (c)

Fig. 2. (a) Antenna array layout with sensors numbering for O-shaped configuration;
(b) corresponding *uv* samples for inter-element spacing $d_A = 1.8\lambda_o$; carrier frequency $f_o = 24$GHz;
(c) relevant PSF for 24 element O-shaped configured imaging array

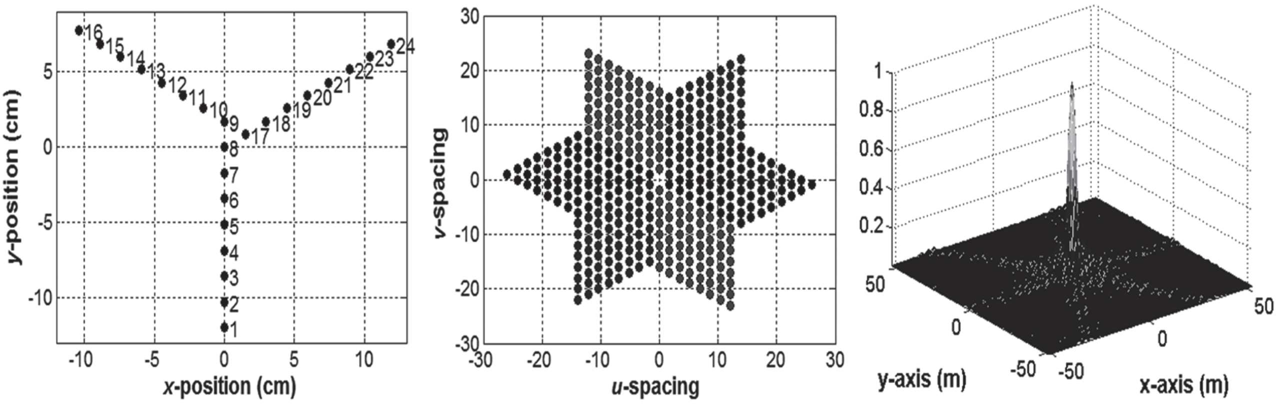

(a) (b) (c)

Fig. 3. (a) Antenna array layout with sensors numbering for Y-shaped GeoSTAR configuration;
(b) corresponding *uv* samples for inter-element spacing $d_A = 1.8\lambda_o$; carrier frequency $f_o = 24$GHz;
(c) relevant PSF for 24 element Y-shaped configured imaging array

III. ENHANCED RADAR IMAGING INVERSE PROBLEM FORMALISM

Following [9], [18] consider the vector-form coherent equation of observation that relates the pixel-framed random scene reflectivity **v** with the coherent array output data signal

$$\{\mathbf{u}(j) = \tilde{\mathbf{S}}\mathbf{v}(j) + \mathbf{n}(j);\ j = 1,\ldots, J\}, \qquad (3)$$

where $\mathbf{n}(j)$ represents the observation noise and $\tilde{\mathbf{S}} = \mathbf{S} + \Delta_{\mathbf{S}}$ is the $M\times K$ ($M < K$ for compressed sensing scenarios) matrix-form approximation of the integral perturbed signal formation operator (SFO), in which the regular component S is specified by the employed radar signal modulation mode specified in Sect. II. Recall that starting from (1) we consider any particular feasible "range gate (r) – polarization mode

(p)" combination $\{r|p\}$, thus omit subscripts $r|p$. In (3), $\mathbf{v}$, $\mathbf{n}$, $\mathbf{u}$ are Gaussian zero-mean vectors composed of the random entries $\{v_k\}_{k=1}^{K}$, $\{n_m\}_{m=1}^{M}$ and $\{u_m\}_{m=1}^{M}$, respectively [9]. These vectors are characterized by the correlation matrices, $\mathbf{R_v} = \mathbf{D}(\mathbf{b}) = diag(\mathbf{b})$, the diagonal matrix with the vector-form SSP b at its principal diagonal, $\mathbf{R_n} = N_0\mathbf{I}$ and $\mathbf{R_u} = <\tilde{\mathbf{S}}\mathbf{R_v}\tilde{\mathbf{S}}^+> + N_0\mathbf{I}$, correspondingly, where the averaging $<\cdot>$ is performed over the randomness of perturbations $\mathbf{\Delta_S}$ of the regular SFO $\mathbf{S}$ in (3), superscript $^+$ stands for Hermitian conjugate, and N_0 is the white observation noise power. Vector $\mathbf{b}$ represents a lexicographically ordered by multi-index $k = (k_x, k_y)$ vector-form approximation of the SSP map $\mathbf{B} = \{b(k_x, k_x)\}$ over the $K_y \times K_x$ pixel-framed 2-D scene $\{k_x = 1,..., K_x;\ k_y = 1,..., K_y;\ k = 1, ..., K = K_xK_y\}$ at each feasible $\{r|p\}$ combination [1].

The feature-enhanced RS imaging problem at hand is to develop the framework (in this study, the unified DEDR-POCS-AB referred to as the DEDR-POCS-restructured MVDR method) and the related technique(s) for high-resolution estimation (feature-enhanced reconstruction) of the SSP

$$\hat{\mathbf{b}} = est_{DEDR\text{-}POCS\text{-}AB}\{\mathbf{b}\,|\,\{\mathbf{u}(j)\};\ j = 1,...,J\} \tag{4}$$

from the available recordings (3) of the complex (coherent) array data $\{\mathbf{u}(j)\}$ degraded by the composite noise (multiplicative $\mathbf{\Delta_S}$ and additive $\mathbf{n}$) with the SFO perturbation statistics $<\tilde{\mathbf{S}}\mathbf{R_v}\tilde{\mathbf{S}}^+>$ usually unknown to the observer.

IV. DEDR RESTRUCTURED MVDR STRATEGY

The high-resolution adaptive estimation of the SSP via the classical adaptive minimum variance distortionless response (MVDR) method [2], [6] employs the strategy

$$\hat{b}_k = \frac{1}{\mathbf{s}_k^+\mathbf{R_u}^{-1}(\mathbf{b})\mathbf{s}_k};\ k = 1,..., K \tag{5}$$

optimal (in the MVDR sense) for the theoretical model-dependent ($\mathbf{b}$-dependent) array covariance matrix inverse $\mathbf{R_u}^{-1}(\mathbf{b})$ where $\mathbf{s}_k^+$ defines the so-called kth steering vector composed of the corresponding kth row ($k = 1,..., K$) of the adjoint regular SFO matrix $\mathbf{S}^+$ [9], [10]. In the real-world RS imaging scenarios, the unknown exact model of the covariance matrix $\mathbf{R_u}(\mathbf{b})$ is substituted by its sample maximum likelihood (ML) estimate [6], [10], [11] $\mathbf{Y} = \hat{\mathbf{R}}_\mathbf{u} = (1/J)\sum_{j=1}^{J}\mathbf{u}(j)\mathbf{u}^+(j)$ (at each treated combination $\{r|p\}$) that yields the conventional MVDR algorithm [2], [6]

$$\hat{b}_k = \frac{1}{\mathbf{s}_k^+\mathbf{Y}^{-1}\mathbf{s}_k};\ k = 1,..., K \tag{6}$$

feasible for the full rank $\mathbf{Y}$ only. From simple algebra, it is easy to corroborate that the theoretical model based strategy (5) is algorithmically equivalent to the solution (with respect to the SSP vector $\mathbf{b}$) of the nonlinear equation

$$\{\mathbf{D}(\mathbf{b})\}_{diag} = \{\mathbf{W}(\mathbf{b})\mathbf{R_u}(\mathbf{b})\mathbf{W}^+(\mathbf{b})\}_{diag} \tag{7}$$

with the solution operator (SO)

$$\mathbf{W}(\mathbf{b}) = (\mathbf{D}(\mathbf{b})\mathbf{S}^+\mathbf{S} + N_0\mathbf{I})^{-1}\mathbf{D}(\mathbf{b})\mathbf{S}^+ . \tag{8}$$

Substituting in (7) the theoretical covariance matrix $\mathbf{R_z}$ by its ML sample estimate $\mathbf{Y} = \hat{\mathbf{R}}_\mathbf{u}$ yields the DEDR-restructured MVDR strategy

$$\hat{\mathbf{b}} \to \text{solution to the Eq.} \to \{\mathbf{D}(\hat{\mathbf{b}})\}_{\text{diag}} = \{\mathbf{W}(\hat{\mathbf{b}})\mathbf{Y}\mathbf{W}^+(\hat{\mathbf{b}})\}_{\text{diag}} \tag{9}$$

or in an equivalent form

$$\hat{\mathbf{b}} \to \text{solution to the Eq.} \to \{\mathbf{D}(\hat{\mathbf{b}})\}_{\text{diag}} = \{\mathbf{K}(\hat{\mathbf{b}})\mathbf{Q}\mathbf{K}^+(\hat{\mathbf{b}})\}_{\text{diag}} \tag{10}$$

with the solution independent sufficient statistics matrix

$$\mathbf{Q} = \mathbf{S}^+\mathbf{Y}\mathbf{S} \tag{11}$$

and the solution dependent matrix-form reconstructive operator

$$\mathbf{K} = \mathbf{K}(\hat{\mathbf{b}}) = (\mathbf{D}(\hat{\mathbf{b}})\Psi + N_0\mathbf{I})^{-1}\mathbf{D}(\hat{\mathbf{b}})\,. \tag{12}$$

Here, we have incorporated the following notations: operator $\{\cdot\}_{\text{diag}}$ returns the vector of the principal diagonal of the embraced matrix, and $\Psi = \mathbf{S}^+\mathbf{S}$ represents the matrix-form point spread function (PSF) of the low-resolution MSF imaging array radar system [9], [18]. Note that matrix $\mathbf{K}$ does not involve inversion of $\mathbf{D}(\hat{\mathbf{b}})$, hence, the DEDR-restructured MVDR strategy (10) results in the desired sparsity preserving technique that admits zero entries in $\mathbf{b}$ and is also feasible for rank deficient data covariance matrices $\mathbf{Y}$ (for $J < M$).

The DEDR framework [8], [9] suggests the worst case statistical performances optimization approach to the problem (4) with the harsh sensing scenario model uncertainties regarding the SFO perturbations that yields the robust SO

$$\mathbf{W}(\hat{\mathbf{b}}) = \mathbf{K}(\hat{\mathbf{b}})\mathbf{S}^+ = (\mathbf{D}(\hat{\mathbf{b}})\Psi + N_\Sigma\mathbf{I})^{-1}\mathbf{D}(\hat{\mathbf{b}})\mathbf{S}^+\,, \tag{13}$$

in which $N_\Sigma = N_0 + \beta$ is the observation noise power N_0 augmented by factor $\beta \geq 0$ adjusted to the regular SFO Loewner ordering factor and the statistical uncertainty bound for the SFO perturbation (see [9] for details). Hence, the robust modification of the DEDR is constructed by replacing in (9), (10) N_0 by the composite $N_\Sigma = N_0 + \beta$ that results in the diagonal loaded $\mathbf{K}$ in (13). In practical scenarios, the loaded regularization factor N_Σ can be evaluated empirically from the noise corrupted low-resolution MSF image following one of the local statistics techniques exemplified in [4], [10].

Solver (10) still contains solution dependent inversions necessary to compute the reconstructive operator (12). Thus, to convert (10) into the solver that avoids *any* matrix inversions, we substitute (10) by the algorithmically equivalent strategy

$$\hat{\mathbf{b}} \to \text{solution to} \to \{\mathbf{A}(\hat{\mathbf{b}})\mathbf{D}(\hat{\mathbf{b}})\mathbf{A}(\hat{\mathbf{b}})\}_{\text{diag}} = \{\mathbf{D}(\hat{\mathbf{b}})\mathbf{Q}\mathbf{D}^+(\hat{\mathbf{b}})\}_{\text{diag}} \tag{14}$$

Next, to modify (14) to the conventional matrix-vector transform form, we make the use of the following properties [9]

Property 1.

$$\{\mathbf{A}(\hat{\mathbf{b}})\mathbf{D}(\hat{\mathbf{b}})\mathbf{A}(\hat{\mathbf{b}})\}_{\text{diag}} = \mathbf{T}(\hat{\mathbf{b}})\hat{\mathbf{b}}\,, \tag{15}$$

$$\mathbf{T}(\hat{\mathbf{b}}) = \mathbf{A}(\hat{\mathbf{b}}) \odot \mathbf{A}^*(\hat{\mathbf{b}}) \tag{16}$$

where $\odot$ defines the Schur-Hadamard (elementwise) matrix product.

Property 2.

$$\{\mathbf{D}(\hat{\mathbf{b}})\mathbf{Q}\mathbf{D}^+(\hat{\mathbf{b}})\}_{\text{diag}} = \mathbf{D}^2(\hat{\mathbf{b}})\mathbf{g}\,, \tag{17}$$

$$\mathbf{g} = \{\mathbf{Q}\}_{\text{diag}}\,. \tag{18}$$

Using these properties, solver (14) is transformed into the following strategy

$$\hat{\mathbf{b}} \to \text{solution to the Eq.} \to \mathbf{T}(\hat{\mathbf{b}})\hat{\mathbf{b}} = \mathbf{D}^2(\hat{\mathbf{b}})\mathbf{g} \tag{19}$$

that does *not* involve *any* matrix inversions, thus guarantees preservation of sparse structures in the desired solution. The latter means that DEDR restructured MVDR strategy (19) is feasible for imaging the scenes composed from extended (spatially distributed) objects as well as scenes composed with some point-type targets (TAGs), i.e., intrinsically sparse scenes, as well as any composite scenes (e.g., point-type TAGs placed over the distrusted extended objects).

The derived solver (19) is extremely nonlinear, hence the desired solution (feature enhanced radar image) can be found only via iterative numerical computing. Now, we are ready to proceed with the development of such a procedure that realizes the DEDR restructured MVDR strategy (19).

V. DEDR-POCS-AB ITERATIVE RI TECHNIQUE

Consider, first, that the SSP estimation formalized by (4) is performed in the positive convex cone solution set $\mathbb{B}_{(K)}$ in the vector space with metric structure specified by some metric inducing operator $\mathcal{M}$ [7], [12], [18]. In the considered in this study standard Euclidean ℓ_2 structured metric, $\mathcal{M} = \mathrm{I}$, i.e., the identity matrix. Other admissible sophisticated metric structures in the solution space that may incorporate image gradient maps and ℓ_1 structured (so-called total variation) metrics [18] are beyond the scope of this paper.

To transform (19) into the iterative feature enhanced RI procedure that performs the desired SSP reconstruction in the solution set $\mathbb{B}_{(K)}$ we incorporate into (19) the composite cascade transform

$$\mathcal{H} = \mathcal{P}_{+\pi}\mathcal{T}\,. \tag{20}$$

Recall that in this study we have adopted the conventional Euclidean ℓ_2 structured metric ($\mathcal{M} = \mathrm{I}$) in the solution space.

The action of such $\mathcal{H}$ is twofold. First, $\mathcal{T}$ transforms (19) into the implicit iterative numerical scheme [17] defined by the canonical contractive mapping equation

$$(1/\tau_{[i]})(\hat{\mathbf{b}}_{[i+1]} - \hat{\mathbf{b}}_{[i]}) + \mathbf{T}_{[i]}(\hat{\mathbf{b}})\hat{\mathbf{b}}_{[i]} = \\ = \mathbf{D}^2(\hat{\mathbf{b}}_{[i]})\mathbf{g};\ i = 0,1,... \tag{21}$$

in which the relaxation parameter $\tau_{[i]}$ must be properly adjusted at each iteration i = 1, ... to guarantee the overall convergence of (21). Instead of such cumbersome (not unique [17]) adjustments of $\tau_{[i]}$, we incorporate into the canonical scheme (21) the POCS operator $\mathcal{P}_{+\pi}$ that serves as a projector onto convex positive solution set $\mathbb{B}_{(K)}$ with standard Euclidean ℓ_2 structured metric ($\mathcal{M} = \mathrm{I}$). Such projector $\mathcal{P}_{+\pi}$ is easily constructed as a hard thresholding operator [11] that at each iteration i = 1, ... clips off all entries of $\hat{\mathbf{b}}_{[i]}$ lower than the user specified nonnegative sparsity preserving tolerance threshold level π. Hence, $\mathcal{P}_{+\pi}$ serves as a convergence guaranteed POCS operator [11] that naturally discards $\tau_{[i]}$ in (21), i.e., one can simply adopt $\tau_{[i]} = 1$ [17]. With such cascade $\mathcal{H}$ the (21) is transformed into the desired implicit iterative feature enhanced DEDR-POCS-AB technique

$$\hat{\mathbf{b}}_{[i+1]} = \hat{\mathbf{b}}_{[i]} + \mathcal{P}_{+\pi}\{\mathbf{D}^2(\hat{\mathbf{b}}_{[i]})\mathbf{g} - \mathbf{T}(\hat{\mathbf{b}}_{[i]})\hat{\mathbf{b}}_{[i]}\};\ i = 1,...,I\,. \tag{22}$$

The iterative process is initialized with the low-resolution incoherent MSF image $\hat{\mathbf{b}}_{[0]} = \mathbf{g}$ formed via (18) and is terminated at $\hat{\mathbf{b}}_{[I]}$ for which the user specified ℓ_2-norm convergence tolerance level ε_{TL} is attained at some $i = I$.

Now, we are ready to outline the iterative DEDR-POCS-AB technique for feature enhanced RI with array radar sensor systems as follows.

Step 1 (*Specifications*)	Specify the model of the imaging radar system by computing its matrix form PSF operator $\Psi = \mathbf{S}^+\mathbf{S}$ specified by the sensor array geometry and employed modulation format defined by the SFO matrix **S**. Specify the operational scenario parameters (the signal formation operator uncertainty bound η, observation noise power N_0, and image prior gray level b_0) that define the amount of the DEDR regularization ($N_\Sigma = N_0 + b_0\eta$), or evaluate factor N_Σ empirically from the low resolution MSF image, e.g., applying any of the local statistics methods exemplified in [4], [10].
Step 2 (*Initialization*)	Initialize the SSP $\hat{\mathbf{b}}_{[0]}$ as an output **g** of the low resolution MSF technique, e.g., 2-D discrete-form FFT (2), specified in the vector-form as $\hat{\mathbf{b}}_{[0]} = \mathrm{g}$ (18). Construct the diagonal matrix-form stabilizer $\mathbf{D}^2(\hat{\mathbf{b}}_{[0]})$ and the corresponding matrices $\mathbf{A}(\hat{\mathbf{b}}_{[0]})$, $\mathbf{T}(\hat{\mathbf{b}}_{[0]})$ that specify the discrepancy term in (22) at the zero step (i = 0) iteration $\hat{\mathbf{b}}_{[0]} = \mathbf{g}$.
Step 3 (*Iterations*)	Run the implicit contractive mapping algorithm (22) repeatedly for iterations i = 1, 2, ...
Step 4 (*Termination*)	Proceed with iterating (22) until the ℓ_2 norm of the difference between two consecutive reconstructions becomes smaller than the user-specified threshold (convergence tolerance level ε_{TL}). In this study, we adopt $\varepsilon_{TL} = 0.05$.

VI. SIMULATIONS AND DISCUSSIONS

In this Section, we corroborate the effectiveness of the proposed iterative DEDR-POCS-AB technique (22) for feature enhanced RI with the particular array radar HW sensor system model featured in our previous study [1]. Referring to that accompanied paper [1], we compared three competing 24-element array geometries with the corresponding layouts featured in Figures 1, 2, and 3. The nominal test scene relates to the range gate r = 30m and was composed of 5 TAGs located at the x-y coordinates (in meters): {0m-0m; 4.5m-6m; 9m-12m; 4.5m-6m; -4.5m-12m}. The harsh sensing scenario with signal-to-noise ratio, SNR = 10 dB was treated in the simulations reported in Figure 4. The original low resolution MSF images (for three feasible treated array configurations) $\hat{b}_{MSF}(\theta_x, \theta_y) = g(\theta_x, \theta_y)$ of the test multiple target scene formed in the 60° cone field of view (FOW) were computed using the 2-D Fourier transform-based MSF procedure (2) implemented in the 2-D discrete-form FFT. The corresponding MSF outputs (2) configured in a lexographical order [11], [18] $\hat{\mathbf{b}}_{MSF} = \mathbf{g}$ (for three treated sensor array geometries: X-, O-, and Y-shaped 24-element arrays) were used to initialize the feature enhancing post-processing (22) as its zero-step iteration $\hat{\mathbf{b}}_{[0]} = \mathbf{g} = \hat{\mathbf{b}}_{MSF}$. The *Specifications* and *Initialization* steps of (22) were computed following the algorithmic outlines detailed above in the previous Section. The corresponding simulation protocols are presented in Figure 4.

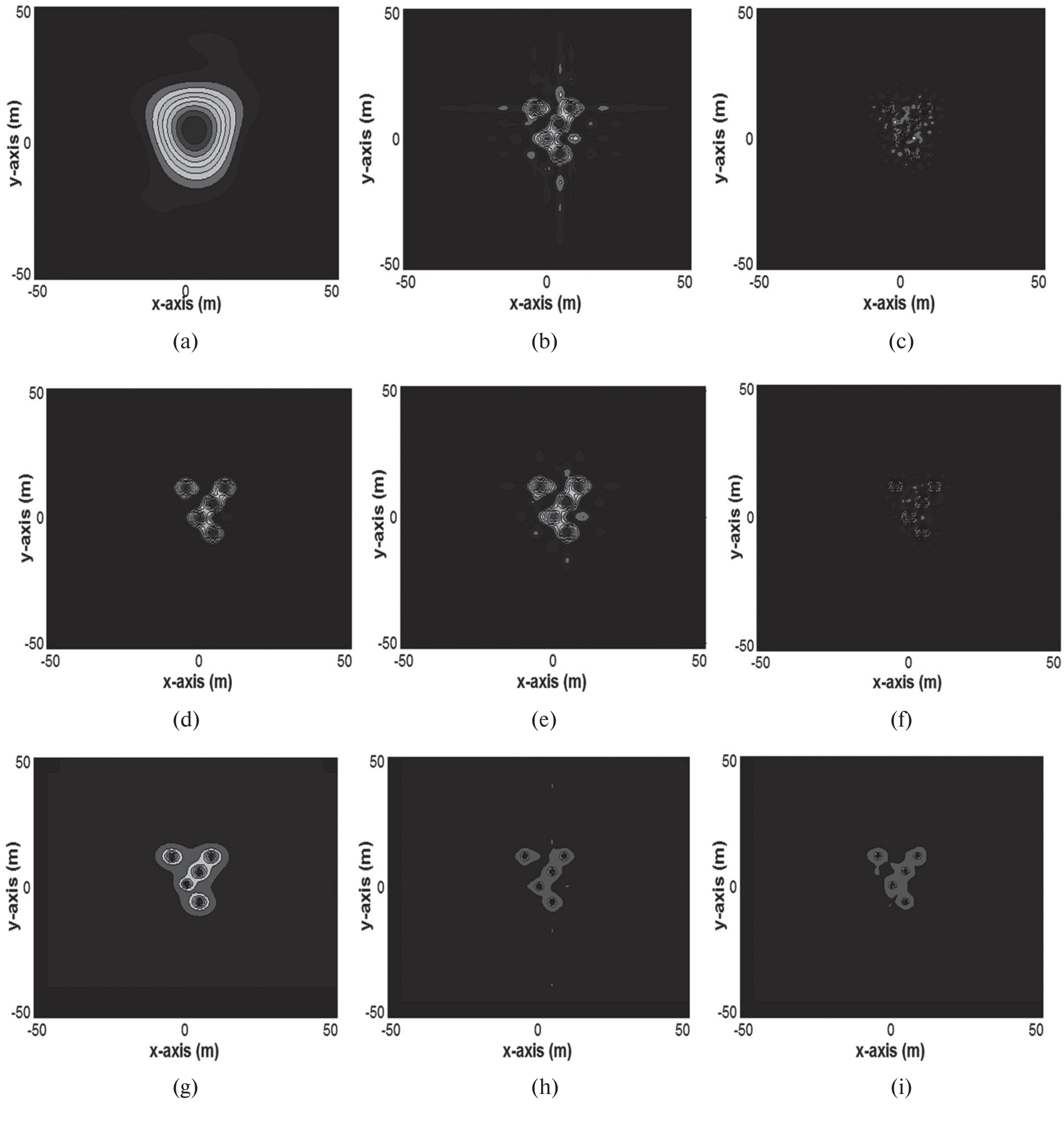

Fig. 4. Multiple target scene RI protocols: (a)-(c) scene image in the (r = 30m range gate) x-y plane formed with the O-, X- and Y-configured imaging array radar systems, respectively, via implementing the conventional DEDR-related low resolution (LR) MSF technique (2); (d)-(f) the same scene images formed with the high resolution (HR) robust version [6] of the classical AB-based method (6); (g)-(i) images formed employing the new DEDR-POCS-AB technique (22)

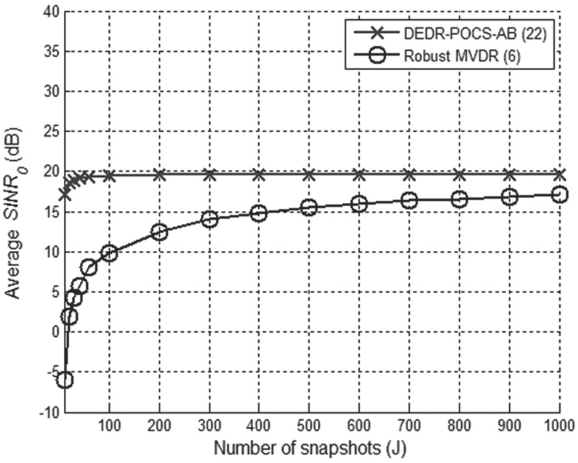

Fig. 5. Comparison of the DEDR-POCS-AB technique (22) and the competing robust HR method [6] in the SINR metrics for the 1st TAG (located in the origin of the scene coordinate system) for SNR = 0 dB

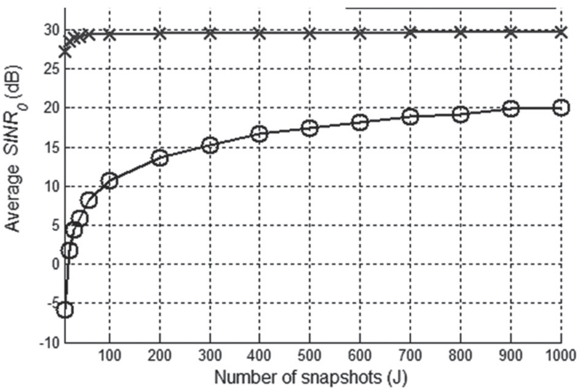

Fig. 6. Comparison of the DEDR-POCS-AB technique (22) and the competing robust HR method [6] in the SINR metrics for the 1st TAG (located in the origin of the scene coordinate system) for SNR = 10 dB

In Figures 5 and 6, we report the signal-to-interference-to-noise ratio (SINR) metrics [6] computed for the 1st (reference) TAG, in which case four other TADs are treated as composite interference sources. Figure 5 reports the low SNR = 0 dB scenario. Figure 6 reports the high SNR = 10 dB scenario. To be comparable with the most prominent competing high resolution (HR) robust MVDR inspired methods in the literature [2], [6], the (22) was run for the worst-case zero-level threshold (i.e., $\pi = 0$) in $\mathcal{P}_{+0}$.

From the reported simulation protocols, the advantage of the most prominent competing MVDR inspired robust AB-based RI techniques (robust version of (6) from [2], [6]) and (22) over the conventional DEDR-related low resolution MSF radar imaging procedure (2) is evident for all three tested array sensor system configurations. In all cases, the best resolution performances and SINRs were manifested by the new proposed DEDR-POCS-AB technique (22). Also, the computational burden of the DEDR-POCS-AB algorithm (22) is usually lower than that of the competing robust adaptive AB-based techniques [2], [6], [18], [19]. We explain this due to avoiding high dimensional ($M \times M \geq 24 \times 24$) data covariance matrix inversions (needed to be computed in each of R_r range gates at each feasible $\{r|p\}$ combination) as well as *any* other matrix inversions in (22). Typically, matrix inversions consume two orders greater number of numerical operations than matrix multiplications (if no "fast" algorithms exist) [17]. In all tested scenarios, the DEDR-POCS-AB algorithm (22) demonstrated asymptotic convergence at ~10 iterations only for the adopted convergence tolerance level $\varepsilon_{TL} = 0.05$. Hence, the computational complexity of the developed iterative algorithm (22) is ~ one order lower than of the regularized robust versions [2], [6], [18] of (6) that involve cumbersome matrix inversions. Moreover, the DEDR-POCS-AB technique (22) is applicable even for the rank-deficient ($J < M$) scenarios, in which the competing methods fail to operate.

VII. CONCLUSION

The radar imaging technique developed in this paper can be interpreted as a novel approach to feature enhanced nonparametric array sensor imaging and spatial spectral analysis with multi-level HW-SW optimization-regularization. The HW co-design level is aimed at the optimization of the array sensor geometry. Our study revealed that in all operational scenarios the drastically superior operational efficiency was attained for the Y-shaped GeoSTAR configured sensor array with the operational characteristics featured in the previous companion paper [1]. At the SW co-design (the algorithm design) level, the novel contribution consists in unification of the recently developed DEDR framework with the sparsity preserving and convergence guaranteed regularizing POCS paradigm. Such unification admits the development of the overall implicit iterative feature enhanced RI procedure that avoids cumbersome matrix inversions at *all* processing stages. The latter decreases the computational cost and allows for effective complexity/performance tradeoff. Moreover, the unified DEDR-POCS-AB approach requires no new HW components, does not need the observer's supervision and is particularly adapted for real-time array radar imaging in harsh sensing environments.

The perspective developments of this study relate to applications of the proposed framework and the developed DEDR-POCS-AB-based signal and image processing techniques to alternative application areas such as multimode spatial analysis, intelligent sensor array and data fusion, dynamic image discrimination for resource management, remote sensing image perception, classification and understanding, etc. This will push forward our capabilities in the multilevel HW-SW co-design-based optimization of the remote sensing RI systems paving a way towards adaptive superresolution sensing performed simultaneously in multiple aggregated wavebands at multiple polarization modalities.

References

[1] *V.E. Espadas and Yu.V. Shkvarko*, "Descriptive Experiment Design Framework for High Resolution Imaging with Multimode Array Radar Systems", *Applied Radio Electronics*, Vol. 12, No.1, pp. 157-165, 2013.

[2] *Jian Li and Petre Stoica.* Robust Adaptive Beamforming. John Wiley & Sons Ltd, 2006.

[3] *F.M. Henderson and A. V. Lewis*, Eds, Principles and Applications of Imaging Radar, Manual of Remote Sensing, 3d ed., vol. 3, NY: Willey, 1998.

[4] *A. Ishimary,* Wave Propagation and Scattering in Random Media. NY: IEEE Press, 1997.

[5] *A.B. Tanner et al,* "Initial Results of the Geosynchronous Synthetic Thinned Aperture Radiometer (GeoSTAR)", IEEE Inern. Symposium on Geoscience and Remote Sensing, IEEE IGARSS 2006, ISBN 0-7803-9510-7/06, pp. 3951-3954, 2006.

[6] *A.B. Gershman,* "Robustness issues in adaptive beamforming and high-resolution direction finding," in High-Resolution and Robust Signal Processing, Yihgo Hua, A.B. Gershman, and Qi Chen Eds., NY- Basel: Marcel Dekker, 2004.

[7] Y. Shkvarko, "Estimation of wavefield power distribution in the remotely sensed environment: Bayesian maximum entropy approach", IEEE Trans. Signal Proc., vol. 50, No. 9, pp. 2333-2346, 2002.

[8] *Y. Shkvarko,* "Unifying regularization and Bayesian estimation methods for enhanced imaging with remotely sensed data—Part I: Theory", IEEE Trans. Geoscience and Remote Sensing, vol. 42, No. 5, pp. 923-931, 2004.

[9] *Y. Shkvarko,* "Unifying experiment design and convex regularization techniques for enhanced imaging with uncertain remote sensing data—Part I: Theory", IEEE Trans. Geoscience and Remote Sensing, vol. 48, No. 1, pp. 82-111, 2010.

[10] *Y.V. Shkvarko,* "Unifying experiment design and convex regularization techniques for enhanced imaging with uncertain remote sensing data ——Part II: Adaptive implementation and performance issues", IEEE Trans. Geoscience and Remote Sensing, vol. 48, No. 1, pp. 96-111, 2010.

[11] *H.H. Barrett and K.J. Myers,* Foundations of Image Science, NY: Willey, 2004.

[12] *S.W. Perry, H.S. Wong, and L. Guan,* Adaptive Image Processing, NY: CRS Press, 2001.

[13] *J.C. Curlander and R. McDonough*, Synthetic Aperture Radar——System and Signal Processing. NY: Wiley, 1991..

[14] *D.R. Wehner,* High-Resolution Radar, 2nd ed., Boston, MA: Artech House, 1994.

[15] *Y. Shkvarko, V. Espadas, and D. Castro,* "Descriptive Experiment Design Optimization of GeoSTAR Configured Multisensor Imaging Radar", 4th International Radio Electronics Forum (4th IREF'2011), Kharkov, Ukraine, Vol. I, pp. 76-81, Oct. 2011.

[16] *Y.V. Shkvarko, J. Tuxpan, and S.R. Santos,* "High-resolution imaging with uncertain radar measurement data: A doubly regularized compressive sensing experiment design approach", in Proc. IEEE 2012 IGARS Symposium, pp. 6976-6970, Munich, Germany, July 2012.

[17] *J.H. Mathews,* Numerical Methods for Mathematics, Science, and Engineering, Second Edition, Englewood Cliffs, NJ: Prentice Hall, 1992.

[18] *Y. Shkvarko,* Jose Tuxpan and Stewart Santos "Dynamic Experiment Design Regularization Approach to Adaptive Imaging with Array Radar/SAR Sensor Systems", Sensors, 11(5):4483-4511, 2011.

[19] *V. Ponomaryov, A. Rosales, F. Gallegos, and I. Loboda,* "Adaptive vector directional filters to process multichannel images", IEICE Trans. Communications, vol. E90-B, No. 2, pp. 429–430, Feb. 2007.

Manuscript received January, 15, 2014

Yuriy V. Shkvarko (M'95–SM'04) received the Dip. Eng. (Hon.) degree in electrical engineering, the Ph.D. degree in radio engineering, and the Dr. Sci. degree in radio physics, radar, and navigation from the Kharkov Aviation Institute, Kharkov, Ukraine, in 1976, 1980, and 1990, respectively. From 1980 to 1991, he was with the Scientific Research Department of the Kharkov Aviation Institute (presently National Aerospace University of Ukraine), as a Research Fellow, a Senior Fellow, and a Chair of the Research Laboratory in information technologies for radar and navigation. From 1991 to 1999, he was a Full Professor with the Department of System Analysis and Control at the Ukrainian National Polytechnic Institute, Kharkov. From 1999 to 2001 he was an Invited Professor with the Guanajuato State University at Salamanca, Mexico. Since 2001, he has been with the Center for Superior Education and Research of the National Polytechnic Institute of Mexico, Guadalajara, Mexico, as a Full Research Professor. He holds 12 patents and has published two books and some 170 international journal and conference papers. His research interests are in applications of signal processing to remote sensing, imaging radar, navigation, and communications, particularly in inverse problems, random fields estimation, robust adaptive spatial analysis, statistical sensor array and multimode remote sensing data processing, and system fusion.

V. E. Espadas (S'10) was born in Mérida, Yucatán, Mexico, in 1985. He received his B.S degree in Electronic Engineering from the Institute of Technology of Merida (ITM), Mexico, in 2008 and the M.S. degree from the Center for Superior Education and Research of the National Polytechnic Institute of Mexico, (CINVESTAV-IPN), Guadalajara, Mexico, in 2011. He is currently working towards the Ph.D. degree at the Department of Electrical Engineering, Telecommunications Division, at the CINVESTAV-IPN. His research interests are in applications of signal processing to remote sensing, radar imaging, statistical sensor array data processing and communications.

D. E. Castro-Palazuelos (S'11) was born in Culiacan, Sinaloa, Mexico, in 1977. He received his B.S. degree in Electronic Engineering from the Institute of Technology of Culiacan (ITC), Culiacan, Mexico, in 2000 and the M.S. degree in Telematics from Colima University, Colima, Mexico, in 2004. He is currently working towards the Ph.D. degree at the Department of Electrical Engineering, Teleommunications Division, at the CINVESTAV-IPN (Center for Superior Education and Research of the National Polytechnic Institute of Mexico), Guadalajara, Mexico. His research interests are in applications of signal processing to remote sensing with parallel data processing, and hardware-software co-design for multimode sensing and communications systems.

УДК 621.396

Альтернативный подход к формированию высококачественных радиоизображений на основе дескриптивной регуляризации процедур диаграмообразования в РЛС с адаптивными антенными решетками / Ю. В. Шкварко, В. Э. Эспадас, Д. Е. Кастро // Прикладная радиоэлектроника: научн-техн. журнал. — 2014. — Том 13. — № 1. — С. 10–19.

Развит альтернативный подход к решению обратных задач формирования высокоразрешающих радиолокационных изображений (РИ) в РЛС с адаптивными антенными решетками на основе концепции многоуровневого дескриптивного планирования эксперимента (ДПЭ). На первом уровне ДПЭ косвенно реализует адаптивное робастное диаграмообразование (ДО) в РЛС с адаптивной антенной решеткой со специальной предложенной «ГеоСТАР» конфигурацией, что позволяет оптимально сбалансировать повышение разрешения с фильтрацией помех. При этом обработка реализуется в итеративной адаптивной форме, исключающей все процедуры инвертирования матриц на всех этапах ДО и формирования результирующих высокоразрешающих РИ. Входными данными служит низкоразрешающее РИ, сформированное стандартным методом согласованной пространственной фильтрации. Для гарантирования сходимости итерационных схем восстановления РИ в исходный метод ДПЭ вводится дополнительный регуляризационый уровень – проекции на выпуклое множество решений (ПВМР) удовлетворяющее накладываемым специальным ограничениям на положительность, пространственную распределенность либо наоборот сосредоточенность объектов, составляющих сцены результирующих РИ. Численное моделирование и сопоставление с конкурирующими методами формирования высокоразрешающих РИ на основе робастных процедур адаптивного ДО в РЛС с антенными решетками подтверждают эффективность предложенного комплексного ДПЭ-ПВМР метода.

Ключевые слова: антенная решетка, дескриптивное планирование эксперимента, РЛС формирования радиоизображений, итеративная обработка, регуляризация.

Рис.: 6. Библиогр.: 19 назв.

УДК 621.396

Альтернативний підхід до формування високоякісних радіозображень на основі дескриптивної регуляризації процедур діаграмостворення в РЛС з адаптивними антенними решітками / Ю. В. Шкварко, В. Е. Еспадас, Д. Е. Кастро // Прикладна радіоелектроніка: наук.-техн. журнал. — 2014. — Том 13. — № 1. — С. 10–19.

Розвинений альтернативний підхід до вирішення зворотних завдань формування високорозподільних радіолокаційних зображень (РЗ) в РЛС з адаптивними антенними решітками на основі концепції багаторівневого дескриптивного планування експерименту (ДПЕ). На першому рівні ДПЕ побічно реалізує адаптивне робасте діаграмо-створення (ДС) в РЛС з адаптивною антенною решіткою зі спеціальною запропонованою «ГеоСТАР» конфігурацією, що дозволяє оптимально збалансувати підвищення розподілу з фільтрацією завад. При цьому обробка реалізується в ітеративній адаптивной формі, яка виключає всі процедури інвертування матриць на всіх етапах ДС і формування результуючих високорозподільних РЗ. Вхідними даними є низькорозподільне РЗ, що сформоване стандартним методом узгодженої просторової фільтрації. Для гарантування збіжності ітераційних схем відновлення РЗ у початковий метод ДПЕ вводиться додатковий регуляризаційний рівень – проекції на випуклу безліч рішень (ПВБР), що задовольняє спеціальним обмеженням, що накладаються на позитивність, просторову розподіленість або навпаки зосередженість об'єктів, що становлять сцени результуючих РЗ. Чисельне моделювання та зіставлення з конкуруючими методами формування високорозподільних РЗ на основі робасних процедур адаптивного ДС в РЛС з антенними решітками підтверджують ефективність запропонованого комплексного ДПЕ-ПВБР методу.

Ключові слова: антенна решітка, дескриптивне планування експерименту, РЛС формування радіозображень, ітеративна обробка, регуляризація.

Іл.: 6. Бібліогр.: 19 найм.